Modulation codes and data processing for seismic apparition of towed-streamer seismic data

Sergio Grion, Daniel Martin and Stuart Denny, Shearwater GeoServices*

Summary

Seismic apparition uses regular periodic codes for blended acquisitions with airgun source arrays, in contrast with the more commonly used natural or artificial random dithers. The periodic codes act as modulation functions and facilitate isolation of the coded sources. This paper discusses modulation codes and an approach for their optimisation, as well as issues related with processing the data in preparation for apparition de-blending.

Introduction

Seismic apparition (Sjøen Pedersen et al., 2016; Robertsson et al., 2016) allows the de-blending of simultaneously acquired shot gathers. This paper considers a triple-source acquisition of 3D seismic data, where three source arrays are towed by a seismic vessel and activated at each shot location, as opposed to the alternate locations typical of flip-flop acquisitions. In line with the seismic apparition principle, at each shot location the sources are modulated in order to facilitate their separation later while processing the data. Initial de-blending results obtained from this data are discussed in Grion et al., (2018) and in this paper we present improved results.

Un-modulated standard sources generate seismic data that, in the temporal frequency- source wavenumber domain, sit within the signal cone (or signal triangle for 2D transforms) determined by the dispersion relation for events travelling in the water column. In the case of triple-source, the effect of modulation is to shift each modulated source to three wavenumber ranges.

If the data is not aliased, these three ranges define a data vector $\mathbf{d}$ which, for each frequency and spatial location, consists of three elements. These can be calculated from the individual un-modulated sources $\mathbf{s}$ via a modulation matrix $\mathbf{M}$:

$$\mathbf{d} = \mathbf{M}\mathbf{s} \qquad (1)$$

The modulation matrix $\mathbf{M}$ depends on the modulation codes used, and the stability of its inversion is one of the key factors for de-blending success (Amundsen et al., 2018).

Modulation codes

With air-gun arrays, the choice of modulation codes for signal apparition is limited. This means that each of the modulated signal cones is a linear combination of all the sources, and therefore de-modulation requires the solution of the linear system of equations (1). Such solution is possible when the determinant of the matrix of coefficients associated with this linear system of equations is stable in the frequency range of interest.

Amundsen et al. (2018) discuss seismic apparition time modulation codes. In particular, several code examples are given for the triple–source case considered in this paper, including an optimized set of time delays that produce a determinant of $\mathbf{M}$ with approximately constant spectrum amplitude over a frequency range from 1 to 100 Hz. Using the same nomenclature of Amundsen et al. (2018), this set of time delays is

$$\mathbf{T} = \begin{bmatrix} 0 & 11 & 19 \\ 11 & 26 & 20 \\ 19 & 21 & 10 \end{bmatrix} \Delta T \quad (2),$$

where T_{ij} is the time-delay associated with source line j and modulation element i, and $\Delta T = 0.001s$. For a triple-source acquisition there are three modulation elements, as each modulation sequence needs to have a periodicity of three shot points.

Grion et al. (2018) propose using the posterior standard deviation of source separation to compare and evaluate apparition codes, and point out that the use of shifted codes for each source ensures equivalent post-separation standard deviations for the three sources. The posterior standard deviation (see for example Tarantola 2005) is defined as

$$\tilde{\mathbf{C}}_\mathbf{s} = \left(\mathbf{M}^* \mathbf{C}_\mathbf{d}^{-1} \mathbf{M} + \mathbf{C}_\mathbf{s}^{-1}\right)^{-1}, \quad (3)$$

where $\mathbf{C}_\mathbf{d} = \sigma_d \mathbf{I}$ and $\mathbf{C}_\mathbf{s} = \sigma_s \mathbf{I}$ are the prior covariance matrices for $\mathbf{d}$ and $\mathbf{s}$, assumed to be diagonal.

Equal standard deviations for the three sources are not guaranteed for a generic code, such as the code in equation (2). To illustrate this point, Figure 1 shows the determinant (bottom) and posterior standard deviations associated with the time delays in equation (2). The determinant plot is equivalent to Figure 5d of Amundsen et al. (2018). The standard deviations for the three sources are similar but not equivalent.

In Figure 1, $\sigma_d = 0.01$ and $\sigma_s = 1$, and the posterior standard deviation is expressed as percentage of σ_s, so that a value of 100 corresponds to equal prior and posterior standard deviations or, in other words, to deblending failure. The value of σ_d is indicated by a purple line in Figure 1 (top). As an alternative to (1), a set of optimised

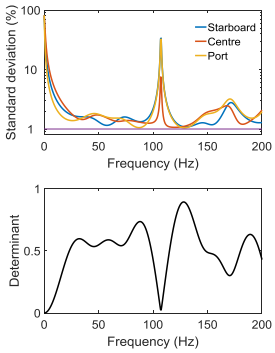

Figure 1: Posterior standard deviation (top) and determinant of the modulation matrix (bottom) for apparition de-blending using the modulation codes of equation (2).

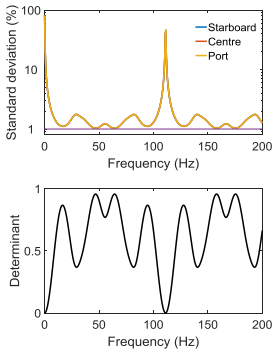

Figure 2: Posterior standard deviation (top) and determinant of the modulation matrix (bottom) for apparition de-blending using the modulation codes of equation (4).

time delays that minimize the posterior standard deviation peak in the range 7-100Hz while at the same time imposing equal posterior standard deviation for the three sources is:

$$\mathbf{T} = \begin{bmatrix} 0 & 21 & 6 \\ 21 & 6 & 0 \\ 6 & 0 & 21 \end{bmatrix} \Delta T. \qquad (4)$$

Figure 2 shows the corresponding determinant and posterior standard deviations. A comparison of Figure 1 and Figure 2 reveals that in both cases the standard deviations are in the range 0-2% in the band of interest, but in Figure 1 the standard deviations differ and this may lead to an acquisition footprint appearing in the separated data.

Besides time-only codes, Grion et al. (2018) consider also joint time and amplitude codes, implemented in practice by periodically switching off some of the guns in each source array. Amplitude codes remain of interest but are not considered in this paper, where we wish to focus on codes optimization strategies and data preparation.

It is interesting to point out that the optimisation strategy need not be limited to peak, average or other statistics of the calculated standard deviations. An additional option is to target specific curves, for example by looking for codes that ensure minimum standard deviation (corresponding to maximum SNR) at frequency bands where source or receiver ghost notches are expected, as a counter-balance to the lower SNR expected in these bands.

Field test

For several years the seismic exploration industry focused on broadband streamer acquisition, testing various sensor configurations and streamer depth profiles. More recently, attention has turned to the source side, with blended and multi-source surveys meant to provide additional flexibility in terms of towing arrangements. Cost, resolution and environmental issues require a range of survey designs that go beyond the conventional flip-flop arrangement with three-string sources. In this context, in September 2017 Shearwater's *Polar Empress* acquired a number of test lines to evaluate various source configuration options, including one line to test seismic apparition with time modulation and one line with joint time and amplitude modulation.

A reference triple-source line was acquired with 12 streamers 75m apart. Source separation was 25m cross-line, with 37.5m in-line between successive shot points for each shot line (i.e. a 12.5 flip-flop-flap acquisition). The apparition lines were acquired with the same streamer spread and the same cross-line source separation but with 18.75m between successive shot points.

The time modulation codes used for the apparition line was, as discussed in Grion et al. 2018,

$$\mathbf{T} = \begin{bmatrix} 8 & 0 & 0 \\ 0 & 8 & 0 \\ 0 & 0 & 8 \end{bmatrix} \Delta T, \qquad (5)$$

and the corresponding posterior standard deviation and determinant are shown in Figure 3. This coding sequence was preferred for its simplicity in a first field implementation of the method, as only one source is delayed at any shot point. However, its peak standard deviation in the range 7-100 Hz is 4% at 7 Hz, double the amount corresponding to the optimized sequence in (4).

The posterior standard deviation in Figure 3 has instabilities at 0Hz and 125Hz. The 125Hz instability is acceptable for the 4ms processing up to 80% of Nyquist (100 Hz) discussed in the next section. At first, the 0Hz instability may appear problematic. It is well known however, that sources close together in time and space act as a single source at low frequencies. Indeed, this is the principle behind the design of air-gun arrays or marine vibrator arrays (Bagaini et al. 2017). The posterior standard deviation of Figures 1-3 depends on modulation codes only, and is independent from the relative position of the shot points. In the case of a triple-source acquisition with a

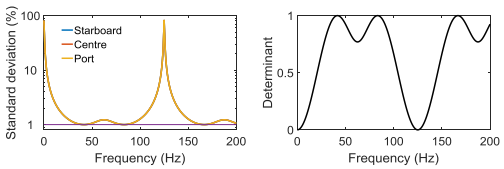

Figure 3: Posterior standard deviation (left) and determinant of the modulation matrix (right) for apparition de-blending using the field test modulation codes of equation (5).

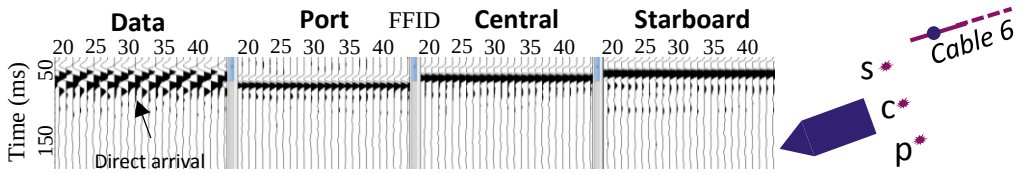

Figure 4: Close-up of a common channel section of apparition data before (left) and after de-blending into port, central and starboard shot lines. The acquisition diagram on the right represents the port (p) , central (c) and starboard (s) sources as well as the near channel (offset 300m) for cable 6 shown in the close up. Before de-blending, the direct arrival has the periodic pattern induced by the modulation. After de-blending this pattern is no longer visible and the the amplitude and arrival time for the direct arrival is as expected from the acquisition diagram, with the starboard source having higher amplitude and reduced traveltime with espect to the other sources.

single boat, the cross-line separation between port, central and starboard sources is small relative to the wavelength at low frequencies, and therefore no de-blending is necessary at those frequencies. Thus the 0Hz instability is not a problem.

Data processing

The acquired apparition data was prepared for seismic apparition de-blending using a careful noise attenuation sequence that included swell noise and tug noise removal, followed by *f-x* interpolation.

For the case of seismic apparition with $n=3$ sources the aliasing frequency is reduced by a factor of $1/3$; and where aliasing is present separation results will be degraded. Aliasing was reduced by first interpolating the data by a factor of four individually for each shot point type ([*8*,0,0], [0,*8*,0] and [0,0,*8*]), in common channels. The three interpolation results were then joined, and apparition de-blending applied. After de-blending, the interpolated traces were dropped to restore the original shot sampling.

Further data preparation included a time-variant wavenumber filtering in common channel, to take into account that at low frequencies the three sources are equivalent to a single, higher volume source and that the data frequency content naturally decays over time.

Figure 4 shows a close-up from a common channel section of the apparition data, before and after de-blending. Since, in a common channel section, each trace is from a different shot point, the modulation pattern is clearly visible at this scale, particularly for the direct arrival. Apparition de-blending separates the recorded data into port, central and starboard source lines.

A sample shot record of apparition data is shown in Figure 5 together with corresponding de-blending results for the port, central and starboard source. The de-blending quality appears high at qualitative inspection. Diffractions are present in the input data at about 0.8s travel-time and are preserved by the de-blending process.

Figure 6 shows a common channel section of the reference data acquired without overlapping shots in the time range shown, compared to apparition data before de-blending and after. Two de-blending results are shown, one with interpolation in the processing sequence and the other without. When interpolation is used separation quality increases, for example in the area highlighted in the figure.

Ongoing work

Ongoing work on this experimental data is along two directions. First, alternative interpolation and regularization algorithms are under investigation, with the intent to improve the current *f-x* interpolation results before apparition de-blending. This step needs to include the interpolation of any missing shots, as their absence can break the periodicity that apparition requires. Second, broadband designature and de-ghosting are going to be included in the data processing sequence. In particular, optimized shot-by-shot directional designature (Hargreaves et al. 2016) will be used to remove any variation in the air-gun array signatures, and phase-shift receiver de-ghosting (Grion et al. 2016) will be used to remove perturbations induced by receiver depth variations. Once interpolation, de-signature and de-ghosting are complete, apparition de-blending will be applied to the data, followed by a standard processing and imaging.

Seismic apparition allows the nearly simultaneous acquisition of n shots. It is therefore attractive to consider the application of any shot-record-based processing before apparition de-blending, so that the processing cost is effectively reduced by $1/n$. In particular this applies to de-signature and receiver de-ghosting.

Conclusions

A first test of seismic apparition on towed-streamer data

gives promising results and highlights the benefits and challenges of the method. Modulation codes should be carefully chosen based on the planned processing bandwidth for the data. Data preparation is key to successful separation and needs to address non-source generated noise (e.g. swell noise, tug noise, dead traces) that would otherwise lead to undesired artefacts after separation.

Acknowledgements

The authors are grateful to Wintershall Norge AS for permission to show the real data examples. The seismic apparition method used for this study are discussed in UK Patent Application GB 2545390, applied for by Statoil Petroleum AS. We thank Shearwater's staff and the crew of the *Polar Empress* for their assistance acquiring the test data.

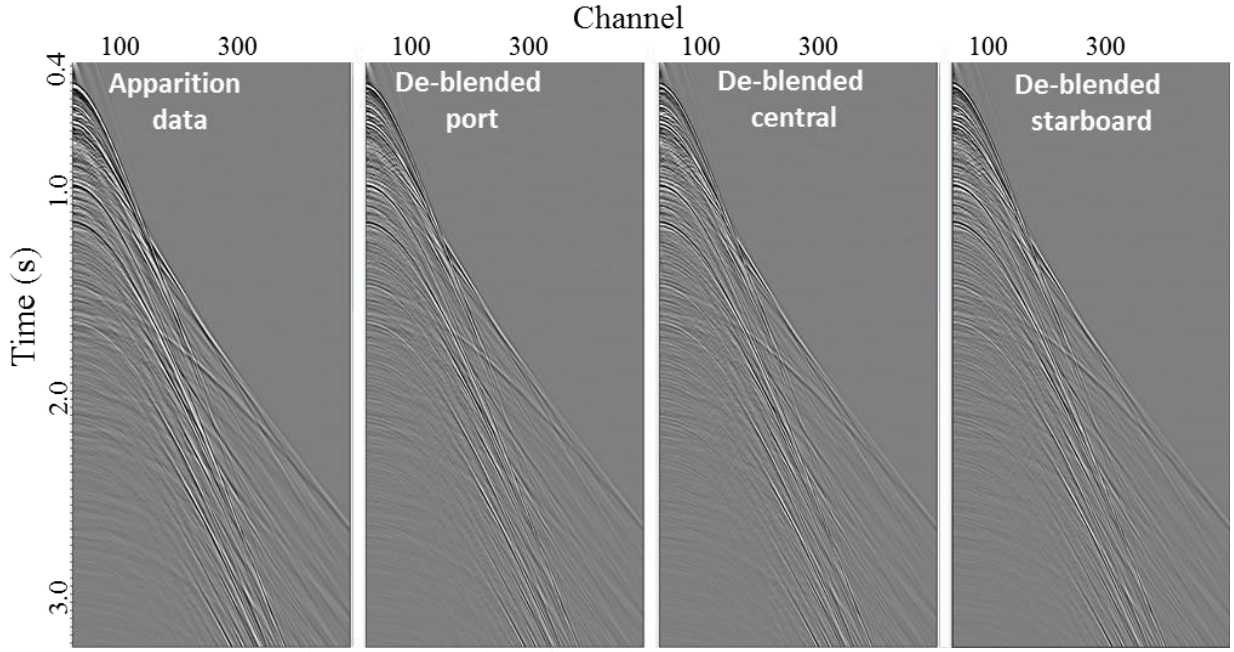

Figure 5: A common shot record of apparition data before (left) and after de-blending into port, central and starboard shots. A qualitative inspection of the results shows that the SNR of the de-blended data is high and comparable to that of the input data.

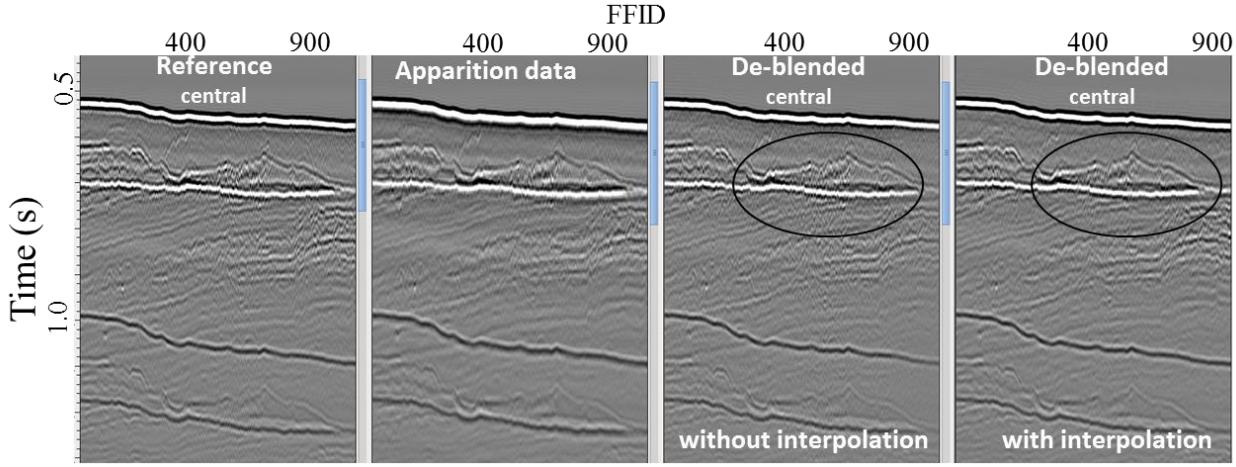

Figure 6: A common channel section from cable 6 of an unblended triple-source reference line (left) is compared to apparition data and apparition de-blending results obtained with and without interpolation. Interpolation improves de-blending results, in particular in the highlighted area.

References

Amundsen, L., Andersson, F., van Manen, D., Robertsson, J.O.A., and K. Eggenberger, 2018, Multisource encoding and decoding using the seismic apparition technique: Geophysics, 83, no. 1, V49-V59.

Bagaini, C., Moldoveanu, N., and I. Moore, 2017, Marine seismic acquisition with phase-controllable sources: 79th EAGE Conference & Exhibition, Extended Abstracts, Tu A4 02.

Grion, S., Telling, R., and S. Holland, 2016, Phase-shift de-ghosting: 78th EAGE Conference & Exhibition, Extended Abstracts, We SRS3 09.

Grion, S., Light, R. and S. Denny, 2018, A seismic apparition experiment on towed streamer seismic data: 80th EAGE Conference & Exhibition Extended Abstracts.

Hargreaves N., Telling R. and S. Grion, 2016, Source de-ghosting and directional designature using near-field derived airgun signatures, 78th EAGE Conference & Exhibition, Extended Abstracts, We SRS3 16.

Robertsson, J.O.A., Amundsen, L., and Å. Sjøen Pedersen, 2016, Wavefield signal apparition part I theory: 78th EAGE Conference & Exhibition, Extended Abstracts, We LHR2 05.

Sjøen Pedersen, Å., Amundsen, L., and J.O.A. Robertsson, 2016, Wavefield signal apparition, Part II: Application to simultaneous sources and their separation: 78th EAGE Conference & Exhibition, Extended Abstracts, We LHR2 06.

Tarantola, A., 2005, Inverse problem theory, SIAM